Flash flood simulations for an Egyptian city - mitigation measures and impact of infiltration

Franziska Tügel[a]*, Ilhan Özgen-Xian[b], Ester Marafini[c], Ahmed Hadidi[d], and Reinhard Hinkelmann[a]

[a]*Technische Universität Berlin, Chair of Water Resources Management and Modeling of Hydrosystems, Gustav-Meyer-Allee 25, 13355 Berlin, Germany,* [b]*EESA, Lawrence Berkeley National Laboratory, Geochemistry Department, Berkeley, California, USA,* [c]*Department of Engineering, Università Degli Studi Roma Tre, Rome, Italy,* [d] *Department of Applied Geosciences, GUtech German University of Technology in Oman, Mucat, Sultanate of Oman*

franziska.tuegel@wahyd.tu-berlin.de

This is an Accepted Manuscript of an article published by Taylor & Francis in Urban Water Journal on 13 January 2020, available online:
http://www.tandfonline.com/10.1080/1573062X.2020.1713171

Flash flood simulations for an Egyptian city - mitigation measures and impact of infiltration

Within this work, the impact of mitigation measures and infiltration on flash floods is investigated by using a 2D robust shallow water model including infiltration with the Green-Ampt model. The results show the combined effects of infiltration and mitigation measures as well as the effectiveness of bypass channels in addition to retention basins. Retention basins at appropriate locations could reduce the maximum water depth at critical locations by 23 %, while the additional implementation of drainage channels lead to a reduction of 75 %, considering also infiltration lead to a further reduction of 97 %. If infiltration was considered without mitigation measures, the peak water depth was reduced by 67 %. For an exceptional extreme event the measures lead to a reduction of 73 % at some locations, while at other locations the overflow from retention basins due to overstraining generated even higher inundations with an increase of 58 %.

Keywords: 2D shallow water model; Hydroinformatics Modeling System; urban flooding; peak flow; infiltration; Green-Ampt model

Subject classification codes: Urban Flood Risk Management: Mitigation and Adaptation Measures in the MENA Region

1. Introduction

Highly developed cities as well as areas with poor infrastructure in different regions all around the world – in arid and humid zones – are often affected by flash floods which are generated by heavy rainfalls. Flash floods often come along with severe damages of infrastructure, houses, and in the worst-case also the loss of human lives leading to economical, ecological and social problems. As their frequency and intensity might increase due to climate change and urbanisation, advanced solutions to mitigate the risk and damages need to be further developed and applied. In arid or semiarid regions, flash floods are often generated by heavy rainfalls in mountainous areas, where huge water volumes are accumulated and quickly transported through wadi systems affecting cities

and infrastructure, which are often located at the wadi deltas, before the water is drained into a water body. The Red Sea region of Egypt is also often affected by flash floods and many cities are not yet protected by structural measures. Measured data from these events are hardly available. Hadidi (2016) carried out and published rainfall and runoff measurements during the flash flood event on 9 March 2014 in El Gouna, a touristic town at the Red Sea coast of Egypt.

In this work, a 2D shallow water model set-up for El Gouna is presented using the measurements from Hadidi (2016) as input. Infiltration excess or so-called Hortonian overland flow is usually the type of runoff generation that occurs during heavy rainfalls in arid areas rather than saturation excess (Blöschl & Sivapalan, 1995). In the model of El Gouna, infiltration processes are considered with the Green-Ampt model, which is one of the most common physically-based approaches to model the temporal development of infiltration. There exist few studies on coupling a 2D shallow water model with the Green-Ampt model, such as Esteves et al. (2000), Singh et al. (2015) and Xing et al. (2019), which generally show good agreements with analytical solutions or measured data and therefore confirm that these methods are capable to simulate rainfall-runoff processes. Simons et al. (2014) already applied the robust shallow water model Hydroinformatics Modeling System (*hms*) with the Green-Ampt model for infiltration, which is used in the present study. They compared the simulation results with a field plot experiment and could show a good agreement with the measurements. *hms* includes robust numerical solution techniques to ensure stability also for very complex flow problems dealing for example with wetting and drying and very small water depths over complex topography, which is the case during rainfall-runoff simulations. The flow model is tested with various benchmarks as well as against experimental data. For further information about *hms* and the implemented robust

numerical methods the following literature is recommended: Hou et al. (2013), Murillo et al. (2009) and Simons et al. (2014).

Some different structural mitigation measures for El Gouna were already investigated within the framework of a master thesis (Marafini, 2017) and are included in the conference contribution of Marafini et al. (2018). In Bauer et al. (2019) a detailed overview of the Wadi Bili catchment is represented.

The research objective of this study is to apply the 2D shallow water model *hms* with consideration of infiltration processes by using the physically-based and time-dependent Green-Ampt model for a combined natural/urban catchment in an arid area. Different structural protection measures to enhance flood mitigation are investigated, while the focus is set on the combined effects of mitigation measures and infiltration processes.

2. Materials and methods

2.1. Shallow water flow model

The Hydroinformatics Modelling Sytem (*hms*) is used to model the flow field generated by the inflow from Wadi Bili and the local rainfall inside the model domain. *hms* was developed at the Chair of Water Resources Management and Modeling of Hydrosystems, Technische Universität Berlin.

The two-dimensional depth-averaged shallow water equations can be written by using the vectors of Equation (2) in the general form of conservation law shown in Equation (1).

$$\frac{\partial \mathbf{q}}{\partial \mathrm{t}} + \frac{\partial \mathbf{f}}{\partial \mathrm{x}} + \frac{\partial \mathbf{g}}{\partial \mathrm{y}} = \mathbf{s} \tag{1}$$

where **q** is the vector of conserved flow variables and t is the time; **f** and **g** denote the

flux vectors in x and y direction, respectively and the vector **s** represents the mass and momentum source terms.

$$\boldsymbol{q} = \begin{bmatrix} h \\ uh \\ vh \end{bmatrix}, \quad \mathbf{f} = \begin{bmatrix} uh \\ uuh + \frac{1}{2}gh^2 - \nu_t \nabla(uh) \\ uvh \end{bmatrix},$$

$$\mathbf{g} = \begin{bmatrix} vh \\ vuh \\ vvh + \frac{1}{2}gh^2 - \nu_t \nabla(vh) \end{bmatrix}, \quad \mathbf{s} = \begin{bmatrix} r \\ -gh\frac{\partial z_B}{\partial x} - f_x \\ -gh\frac{\partial z_B}{\partial y} - f_y \end{bmatrix} \tag{2}$$

where h is the water depth, u and v are the velocity vector components in the x and y directions respectively and z_B is the bottom elevation above datum. r is a mass source/sink term, g is the gravitational acceleration, the turbulent viscosity is denoted with ν_t, and the external forces with f, which includes the bottom friction. In this study, the turbulent viscosity ν_t is set to zero and the bottom friction is calculated with Manning's law, other external forces are not considered. Rainfall and infiltration are considered in the source/sink term in the mass balance equation.

By discretizing the general form of the conservation law with a cell-centred finite–volume method in space and an explicit forward Euler method in time, the conserved variables **q** can be calculated for the new time level n+1 as follows:

$$\mathbf{q}^{n+1} = \mathbf{q}^n - \frac{\Delta t}{A}\sum_k \mathbf{F}_k^n \cdot \mathbf{n}_k l_k + \Delta t \mathbf{s}^n \tag{3}$$

where n+1 and n denote the new and the old time level, respectively, **F** the flux vector over the edge k of the considered cell. The time step is denoted with Δt and A is the area of the considered cell; **n** is the normal vector pointing outward of a face and l is the length of a face.

2.2.Infiltration

There exist various models to include infiltration losses in rainfall-runoff models, which can be basically classified in three groups: 1) physically-based models, 2) semi-empirical models, and 3) empirical models (Gargouri-Ellouze et al., 2017). The standard ϕ-index-method, which is one of the most common empirical approaches, considers a constant loss-rate over the whole event, while the method with an exponentially decreasing infiltration rate is comparable to the temporal development of infiltration rates in the Green-Ampt model depending on the soil moisture. Gargouri-Ellouze & Eslamian (2014) used a statistical approach correlating the ϕ-index with rainfall characteristics to estimate the effective rainfall in ungauged basins.

Besides the more physically-based ground of the Green-Ampt model, a clear advantage compared to the empirical models can be seen in the fact that it is possible to include the effect of higher water depths resulting from a flood wave at some locations and time steps, which leads to higher infiltration rates due to a higher potential gradient.

In the Green-Ampt model the cumulative infiltration and the infiltration rate are calculated with the following equations:

$$F(t) = Kt + (h_0 - \psi)\Delta\theta \ln\left(1 + \frac{F(t)}{(h_0 - \psi)\Delta\theta}\right) \tag{4}$$

$$f(t) = K\left(1 + \frac{(h_0 - \psi)\Delta\theta}{F(t)}\right) = \frac{dF}{dt} \tag{5}$$

where F(t) denotes the cumulative depth of infiltration, f(t) the infiltration rate, K the hydraulic conductivity at residual air saturation, which is assumed to be 50% of the saturated hydraulic conductivity K_s (Whisler & Bouwer, 1970). ψ is the wetting front soil suction head, h_0 the ponding water depth and Δθ the soil moisture deficit, which is the difference between the effective porosity n_{eff} and the initial moisture content θ_i. The

effective porosity, wetting front soil suction head and hydraulic conductivity are called Green-Ampt parameters. Rawls et al. (1983) analysed different soils and developed average Green-Ampt parameters based on soil texture classes, where four of them are shown in Table 1.

Table 1: Green-Ampt parameters after Rawls et al. (1983)

Soil texture class	**Effective porosity n_{eff} (-)**	**Soil suction head ψ (cm)**	**Hydraulic conductivity K (m/s)**
Sand	0.417	4.95	$3.27 \cdot 10^{-5}$
Loamy Sand	0.401	6.13	$8.31 \cdot 10^{-6}$
Sandy Clay Loam	0.330	21.85	$4.17 \cdot 10^{-7}$
Clay loam	0.309	20.88	$2.87 \cdot 10^{-7}$

2.3.Study area

El Gouna is a touristic city in the Eastern Desert of Egypt about 22 km north from Hurghada, with approximately 15.000 inhabitants. The mean elevation is 7 m a.s.l. (Burle, 2018) and the mean annual precipitation of Hurghada, which is the closest city to El Gouna with available long-term rainfall measurements, is about 3 mm/year (Merkel, 2019). The main wadi affecting the city is Wadi Bili, whose catchment area has an extension of approximately 880 km² coming from the Red Sea Mountains and draining into the Red Sea. The wadi crosses the Abu Shar plateau through a steep canyon and spreads into several streams when reaching the coastal plain. The mean slope between the outlet from the Abu Shar plateau and the city of El Gouna is about 5 ‰, which is in addition to the incoming momentum of the flood wave from the moutains the driving force for the flow to propagate in direction to El Gouna. Although several heavy rainfall events already affected different cities in the Red Sea Governorate in terms of severe infrastructure and house damages and loss of human lives, only a few rain gauges are installed along the Red Sea coast and no direct

measurements are available for the remote mountainous areas. Figure 1 shows the location of El Gouna and the catchment area of Wadi Bili up to the outlet of the measured discharge.

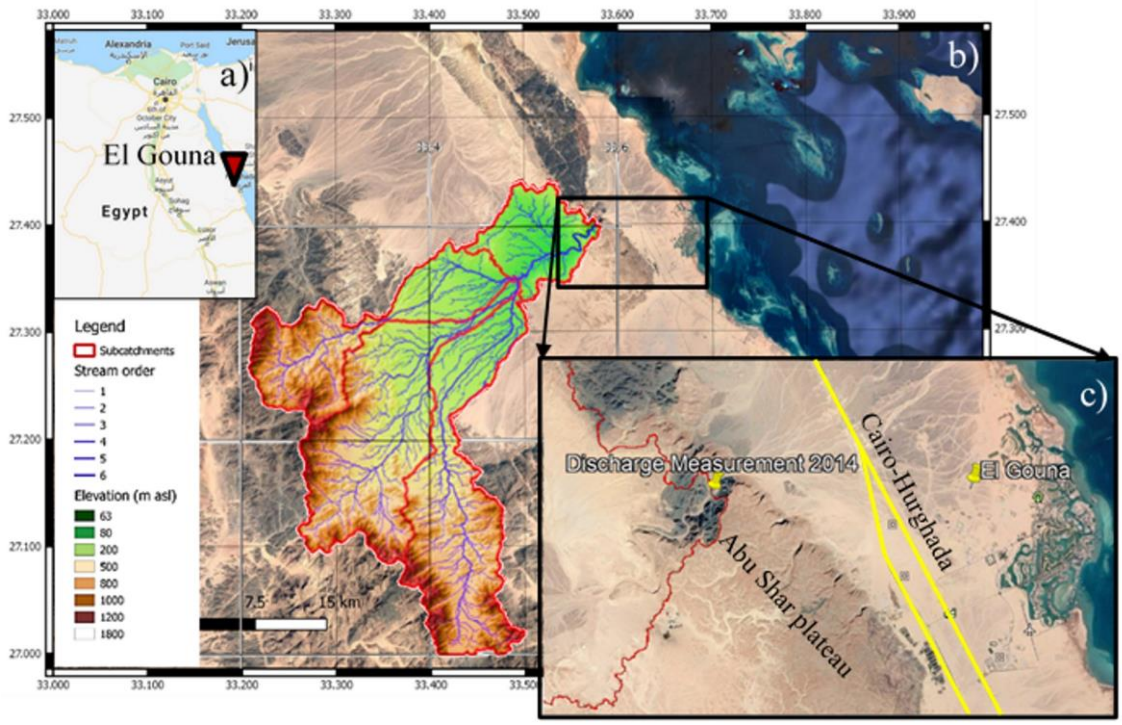

Figure 1: a) Location of Hurghada in Egypt (Map Data ©2017 Google), b) Catchment boundaries, DEM and streams of Wadi Bili, visualized with QGIS, c): location of discharge measurements from Hadidi (2016) and the region of El Gouna inside the wadi delta (Data SIO, NOAA, U.S. Navy, NGA, GEBCO ©2017 ORION-Me, Image ©2017 CNES/Airbus, Image ©2017 Digital Globe)

3. Results and discussion

3.1 Model set-up – computational domain, initial and boundary conditions

To simulate the flow field between the Wadi Bili canyon and the city of El Gouna a model area of approximately 11.3 km x 8 km was chosen. The grid consisted of 403704 rectangular cells with an area of 15 m x 15 m. The digital surface model ALOS WORLD 3D (AVE) was used to represent the topography of the model area. A Manning coefficient of 0.025 $m^{-1/3}$·s was used to represent the friction of a natural, clean channel with no vegetation. The system is considered to be initially dry. All model boundaries were defined as open boundaries except for a 30 m long section at the

western model boundary, where the discharge measurements have been carried out (Figure 1c) and where the inflow hydrograph from Wadi Bili was implemented. For simplicity, the total measured rainfall of 34 mm was considered as equally distributed over a time period of 8 hours when the measurements showed the highest intensities leading to an intensity of 4.25 mm/h. A time period of 43 hours was simulated.

3.2 Simulation scenarios

The simulation with inflow and rainfall from the event in March 2014 and without considering mitigation measures and infiltration is called reference case. In addition to the reference case, twelve different scenarios regarding infiltration, mitigation measures, and accumulated rainfall were simulated. Table 2 gives an overview of all simulated scenarios. Scenarios 1a, 1b and 1c are without any mitigation measure, but with considering infiltration for different soils. In scenarios 1d and 1e the inputs for rainfall and inflow are taken for an accumulated rainfall of 90 mm over the whole catchment area to represent an exceptional extreme event as worst-case scenario. Scenario 2 represents the first mitigation strategy and includes one big retention basin, which is located around one kilometre behind the inflow from Wadi Bili and should capture the whole inflow from Wadi Bili, and two smaller retention basins, which are located behind the main roads of the connection Cairo-Hurghada and should capture the accumulated water generated from the local rainfall around these areas. The locations and numbering of the basins are shown in Figure 2 and the dimensions are given in Table 3. Scenarios 3a, b c, d and e include the same basins as scenario 2 and additionally two channels, where the first one drains the water from basin 3 to basins 2 and the second channel drains the water from basin 2 into the lagoon in the southeast of El Gouna directly north of the airport (see Figure 2). Currently, there are no buildings at

these locations, but the channels cross several roads, where specific solutions such as culverts or bridges must be constructed. These structures are not specifically considered in this work, as the structural measures are just implemented in a simplified way and locations are chosen mainly depending on the flow field of the reference case. The dimensions of the channels are given in Table 3. In scenario 3a infiltration is not considered while 3b and 3c include infiltration for two different soils. In the scenarios 3d and 3e, the inputs of rainfall and inflow hydrograph are used for an accumulated rainfall of 90 mm over the whole catchment area, analogue to scenarios 1d and 1e. While no infiltration is considered in 3d, scenario 3e includes infiltration for sandy clay loam. In scenario 4, the big retention basin close to the outlet from Wadi Bili is substituted by 2 smaller retention basins, which should further reduce the water depths at the crossroad (point E on Figure 3b), where a big inundated area causing road damages and traffic chaos has been observed during heavy rainfall events in that area and where also high water depths have been simulated in the reference case. The locations of these basins are shown in Figure 2 and the dimensions are given in Table 3. A disadvantage of that variant could be that not the whole inflow from Wadi Bili is captured and that the northern parts of the model domain, and specifically the northern parts of the main road Cairo-Hurghada, where a gas station and a police station are located, are not protected by a retention basin or other measures. In this scenario, infiltration is not considered.

Table 2: Overview of different simulation scenarios

		Scenario	Accumulated rainfall	Mitigation measures	Infiltration
Without mitigation measures		Reference case	34 mm	-	no infiltration
		1a	34 mm	-	sandy clay loam, θ_i=0 %
		1b	34 mm	-	loamy sand, θ_i=0.8 %
		1c	34 mm	-	clay loam, θ_i= 3 %
		1d	90 mm	-	no infiltration
		1e	90 mm	-	sandy clay loam, θ_i=0 %
With mitigation measures		2	34 mm	1 big basin + 2 smaller basins without channels	no infiltration
		3a	34 mm	1 big basin + 2 smaller basins with channels	no infiltration
		3b	34 mm	1 big basin + 2 smaller basins with channels	sandy clay loam, θ_i=0 %
		3c	34 mm	1 big basin + 2 smaller basins with channels	clay loam, θ_i= 3 %
		3d	90 mm	1 big basin + 2 smaller basins with channels	no infiltration
		3e	90 mm	1 big basin + 2 smaller basins with channels	sandy clay loam, θ_i=0 %
		4	34 mm	4 smaller basins with channels	no infiltration

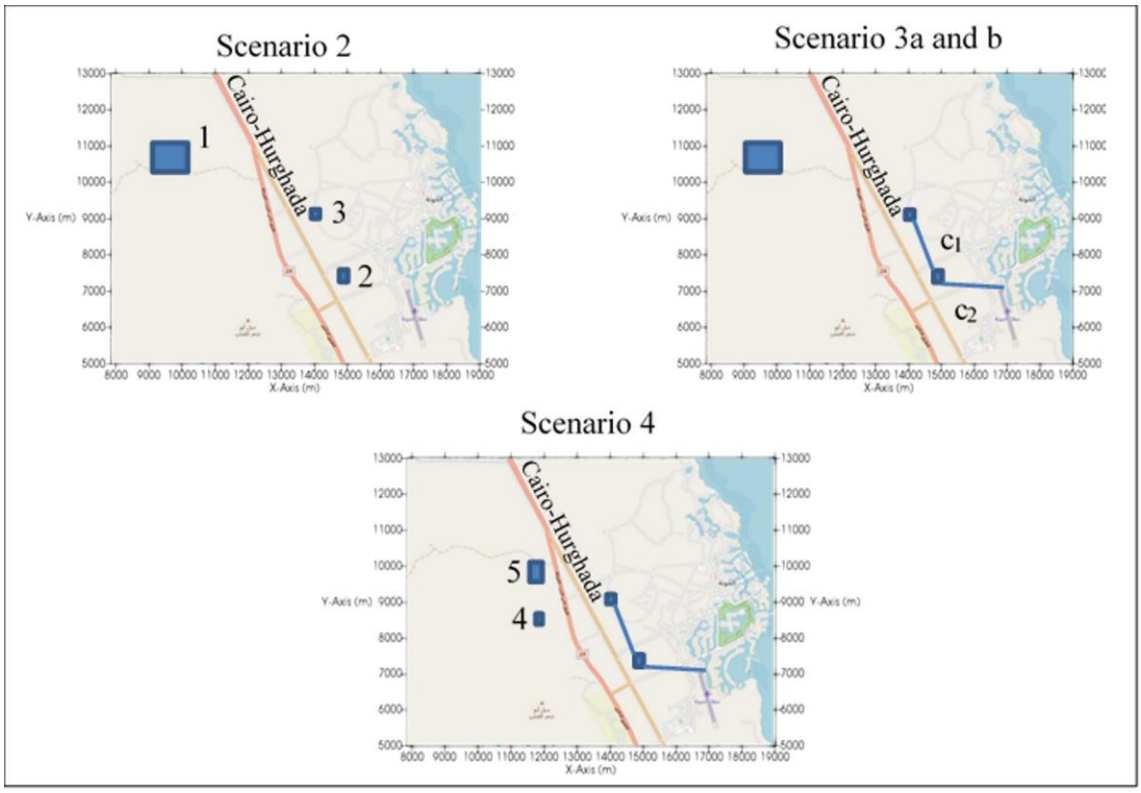

Figure 2: Location and numbering of the different retention basins and channels, plotted on www.openstreetmap.org ©OpenStreetMap contributors

Table 3: Dimensions of basins and channels in the scenarios with mitigation measures

	Nr.	Length (m)	Width (m)	Max. depth (m)	Max. storage volume (million m^3)
Basins	1	1080	800	2.6	2.23
	2	300	390	2.0	0.23
	3	300	300	1.0	0.09
	4	300	240	1.9	0.14
	5	585	400	2.8	0.66
Channels	**Nr.**	**Length (m)**	**Width (m)**	**Max. depth**	**Slope (‰)**
	c_1	1498	60	2.0	2.7
	c_2	2023	60	2.0	2.2

3.3 Comparison of different scenarios

3.3.1. Reference case and infiltration scenarios without mitigation measures

Firstly, the main characteristics of the simulated flow field and the results of the reference case are described, and secondly the impact of infiltration considering two different soils are presented in this section. Figure 3 shows the results of the flow field for the reference case after 9 hours of simulation time in terms of the spatial distribution of flow velocities and water depths in the model domain, plotted on open street maps. This time step was chosen to show the flow propagation exemplarily, because the maximum water depth for the reference case occurred after 9 hours. It can be seen that the flood coming from Wadi Bili spreads into different streams when it reaches the coastal plain. Furthermore, the local rainfall accumulated in some smaller wadis south of the Wadi Bili outlet and the flow propagates in northeast to east directions crossing the main road at X=13000 and Y=8000 (point A in Figure 3b) leading to inundations between the two main roads of up to 20 cm and flow velocities up to 1 m/s. Also, some smaller streams in the north of the city area are generated by local rainfall of the surrounding area and water depth up to 25 cm (point B in Figure 3b) and 30 cm respectively (point C in Figure 3b) occurred. One stream propagating from the Wadi Bili canyon to the northeast is crossing the main road at X=11500 and Y=12000 (point D in Figure 3b), and causing inundations of 25 cm directly south of the gas station. The main stream propagating to the city of El Gouna crosses the main road at X=12500 and Y=9000 and generates inundations of up to 47 cm in the area of the crossroad connecting the two main roads (point E in Figure 3b), where road damages and traffic chaos during rainfall events have been reported. Afterwards, the stream continues with flow velocities up to 1.6 m/s mainly to the southeast in direction of the desalination plant (point F and red circle in Figure 3b). The overall highest simulated water depths of

up to 83 cm occur in the area directly northwest of the desalination plant. East of the lagoon of a cable park, where road and cable damages during the event in March 2014 are documented, and where many new buildings have been constructed in the recent years, water depths up to 55 cm and flow velocities up to 1 m/s were calculated (point G in Figure 3b).

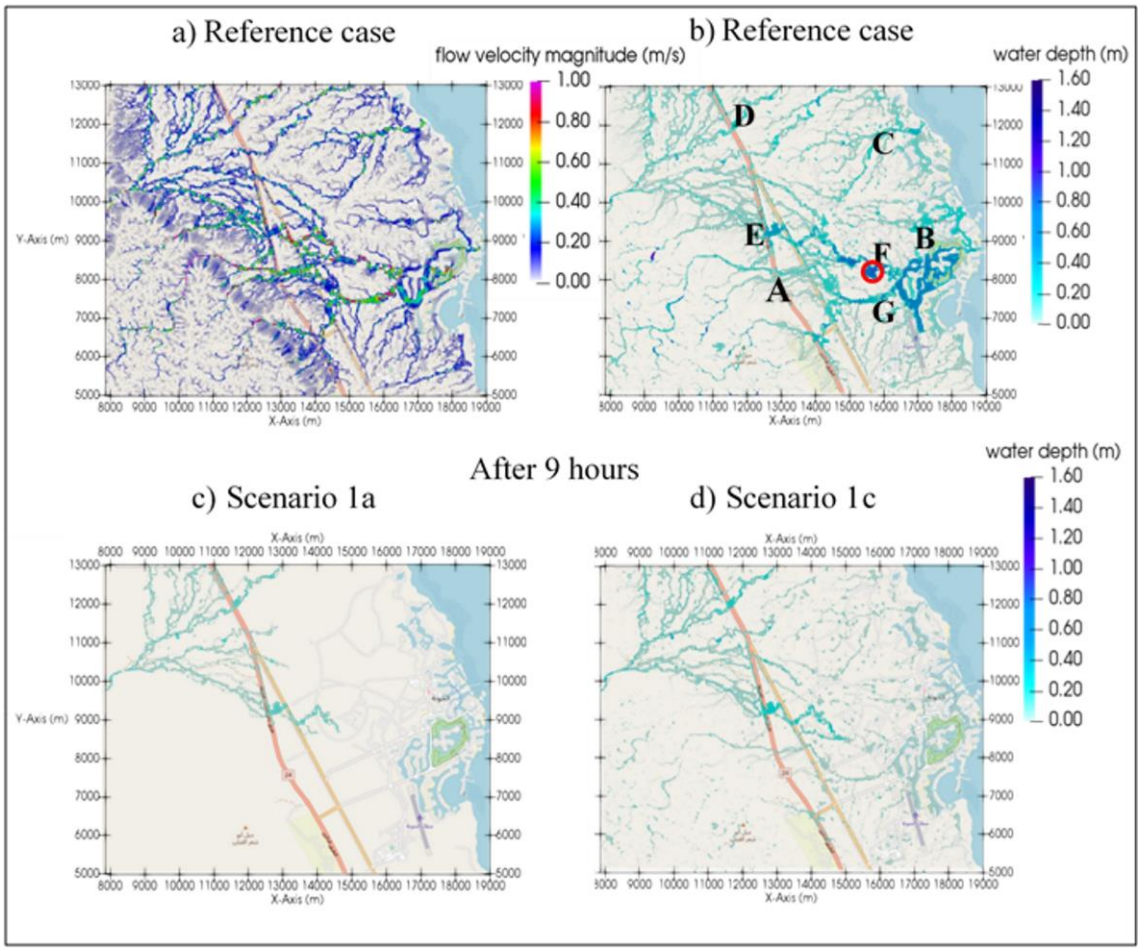

Figure 3: Results after 9 hours of simulation time: a) flow velocities (m/s) of the reference case, b) water depths (m) of the reference case, c) water depths considering sandy clay loam, and d) water depths considering clay loam, plotted on www.openstreetmap.org ©OpenStreetMap contributors

Figure 3c and d show the water depths of scenarios 1a and 1c after 9 hours, considering infiltration for sandy clay loam and an initial moisture content of 0 % on the left side and for clay loam with an initial moisture content of 3 % on the right side. In scenario 1a the local rainfall inside the model domain completely infiltrated and did not

lead to any surface runoff, while in scenario 1c surface runoff generated by the local rain occurred in some areas. The flood wave from Wadi Bili is also strongly reduced and delayed, as in both scenarios the flood did not yet reach the location of maximum water depth in the reference case for the same time step. Scenario 1b with infiltration for loamy sand is not represented in Figure 3, as all the local rain and almost all the water from the inflow from Wadi Bili already infiltrated in the beginning and the flood did not reach any of the considered locations, which becomes clear in Figure 4, where the water depths for the different scenarios is plotted over time at the crossroad (point E in Figure 3b) and at the desalination plant (point F in Figure 3b). The reduction of the water depths in scenario 1a with sandy clay loam and scenario 1c with clay loam compared to the reference case becomes clearly visible at both locations, while the difference between 1a and 1c is more accentuated at the desalination plant (Figure 4 right). The time shift of the flood peak is more clearly visible at the desalination plant, which is located farther from the inflow location than the crossroad. At both locations, no surface runoff occurs for the scenario 1b considering loamy sand.

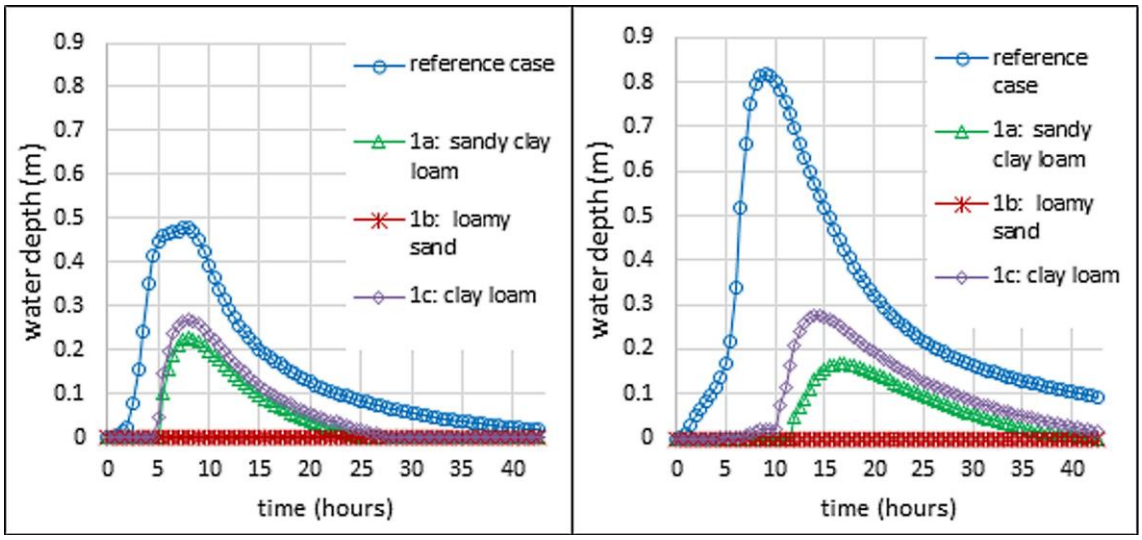

Figure 4: Water depth over time for the reference case and the different infiltration scenarios 1a, 1b, and 1c at the crossroad (left) and close to the desalination plant (right)

3.3.2. Different mitigation measures with and without infiltration

In Figure 5a-d the reference case is compared to the three scenarios 2, 3a and 4 where different mitigation measures were implemented in the model. The big retention basin in the scenarios 2 and 3a decreased the water depths and flooded areas at the northern parts and especially around the gas station (point D in Figure 5a) as well as a bit at the crossroad (point E in Figure 5a). But when comparing the reference case with scenario 2 the water depth reduction at the crossroad is not very big. Therefore, 2 other smaller retention basins were implemented in scenario 4, and they could successfully further reduce the maximum water depth at the crossroad (Figure 6a). On the other hand, the water depths at the northern parts of the road and at the gas station (point D in Figure 5a) could not be reduced with these measures. The two smaller retention basins east of the main roads, which are present in all scenarios, reduced the water depths especially in the area around at the desalination plant (point F in Figure 5a). When comparing the scenarios 2 and 3a it becomes clear that the implementation of the drainage channels could prevent an overflowing of the smaller retention basins and induce a blocking of the flow paths from west to east and a collection of the water between the two smaller basins, which lead to a strong decrease in water depths around the desalination plant (point F in Figure 5a) as well as close to the cable park (point G in Figure 5a).

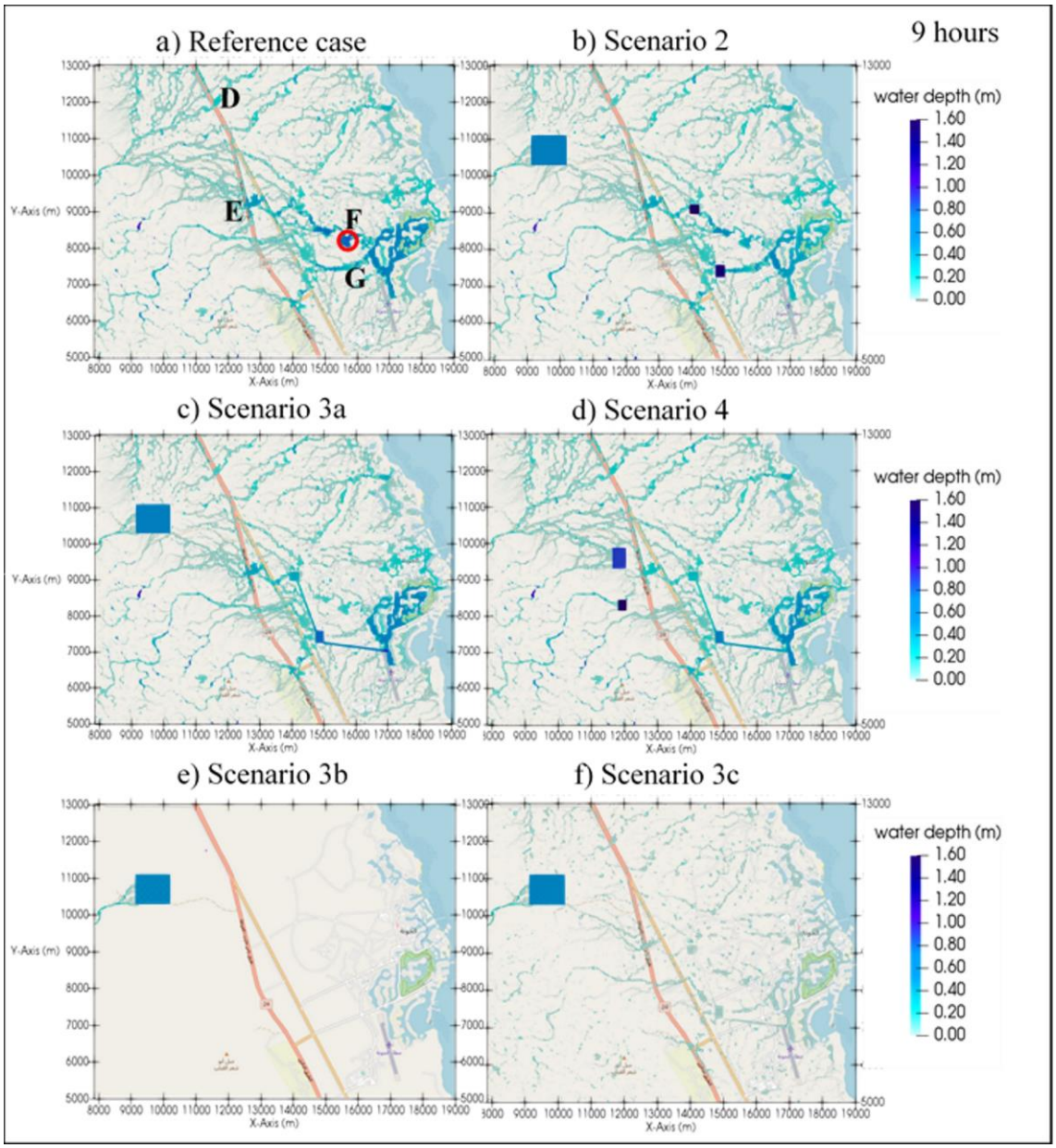

Figure 5: Simulated water depths after 9 hours for the mitigation measures in scenario 2 (with one big and two smaller basins), 3a (with one big and two smaller basins and 2 channels), 4 (with 4 smaller basins and 2 channels), 3b (same mitigation measures as in 3a, but with infiltration for sandy clay loam), and 3c (same mitigation measures but with infiltration for clay loam), plotted on www.openstreetmap.org ©OpenStreetMap contributors

In Figure 6a-c the temporal development of water depth is illustrated for selected locations to analyse the impact of the different mitigation measures more detailed. The peak water depth at the crossroad could be reduced from 48 cm in the reference case to 41 cm (15 %) in scenario 3a and to 30 cm (38 %) in scenario 4. The water depth close to the gas station (point D in Figure 5a) could be reduced from 35 cm in the reference case

to 17 cm (51 %) in scenario 3a, while there was no reduction in scenario 4. To better mitigate the flooding around the gas station (point D in Figure 5a) and at the crossroad (point E in Figure 5a) at the same time, a better option could be to build one smaller retention basin closer to the gas station in addition to the ones in scenario 4. This option was not further investigated here. The maximum water depth in the reference case which occurred next to the desalination plant (point F in Figure 5a) could be reduced from 83 cm to 64 cm (23 %) in scenario 2 with three retention basins, and to 21 cm (75 %) in the scenarios 3a and 4 where channels are implemented additionally to the basins (Figure 2). This strong decrease between scenario 2 without channels compared to the scenarios with channels shows the effectiveness of the channels to mitigate the flooding in the area around the desalination plant (point F in Figure 5a) and the cable park (point G in Figure 5a). The mitigation measures in scenario 3a were chosen to be further investigated in the scenarios 3b and 3c considering infiltration. While in scenario 3b infiltration for sandy clay loam with an initial moisture content of 0 % is taken into account, scenario 3c considers clay loam with an initial moisture content of 3 %. In Figure 5e it becomes clear, that the combination of the mitigation measures with infiltration for sandy clay loam is completely effective leading to no flooding areas in the whole model domain, except for the small region behind the inflow location until reaching the biggest retention basin. This is due to the fact that the local rainfall infiltrates immediately, so that no flow streams are generated by the local rainfall, and the incoming flood wave from Wadi Bili is completely captured in the big retention basin. Regarding the water depths of scenario 3c, the mitigation measures in combination with clay loam are also effective and only small water depths below 20 cm occur inside the model domain (Figure 5f). While the water depth at the crossroad (point E in Figure 5a) reaches 27 cm (44 % reduction) if only infiltration for clay loam

is considered but no mitigation measures (Figure 4), and 41 cm (15 %) for the consideration of mitigation measures but without infiltration in scenario 3a, it was reduced to 3.7 cm (92 %) if infiltration and mitigation measures were considered together (Figure 6a). The same effect can be observed at the desalination plant (point F in Figure 5a), where the peak water depth considering infiltration for clay loam was 27 cm (67 %), and 21 cm (75 %) when taking into account the mitigation measures in scenario 3a, while it was reduced to 2.2 cm (97 %) and over just a very short time period in scenario 3a where infiltration and mitigation measures are taken into account at the same time. Figure 6d illustrates the temporal development of infiltration rates at the crossroad for the different infiltration scenarios shown in Section 3.3.1 and for scenario 3c with mitigation measures and infiltration for clay loam. In the beginning, the infiltration rates for all scenarios are as big as the rainfall intensity, thus all soils are absorbing the complete rainfall in the first hours. For the scenarios 1c and 3c, the rates start to drop after 4 hours, as the infiltration capacities are reduced due to the decreased soil moisture deficit (Equation 5). After 4.5 hours, the flood wave reaches the location and the increased ponding water depths lead to increased infiltration rates in scenarios 1a and 1b, which afterwards gradually decrease with progressing time. In scenario 1c all water from the flood wave already infiltrated before it could reach that location, therefore the infiltration rates remain the same as the rainfall intensity until the rain stops after 8 hours. In scenario 3c, the infiltration rate further decreased after 4 hours, as the flood wave was damped by mitigation measures and the ponding water depth is not high enough to compensate the decreased moisture deficit. When the rates immediately drop to zero, it indicates that there is no more water available and thus the area is not flooded anymore. For clay loam this occurs after 28.5 hours, for sandy clay loam after

25.5 hours, for clay loam with mitigation measures after 19 hours and for loamy sand directly when the rain stops after 8 hours.

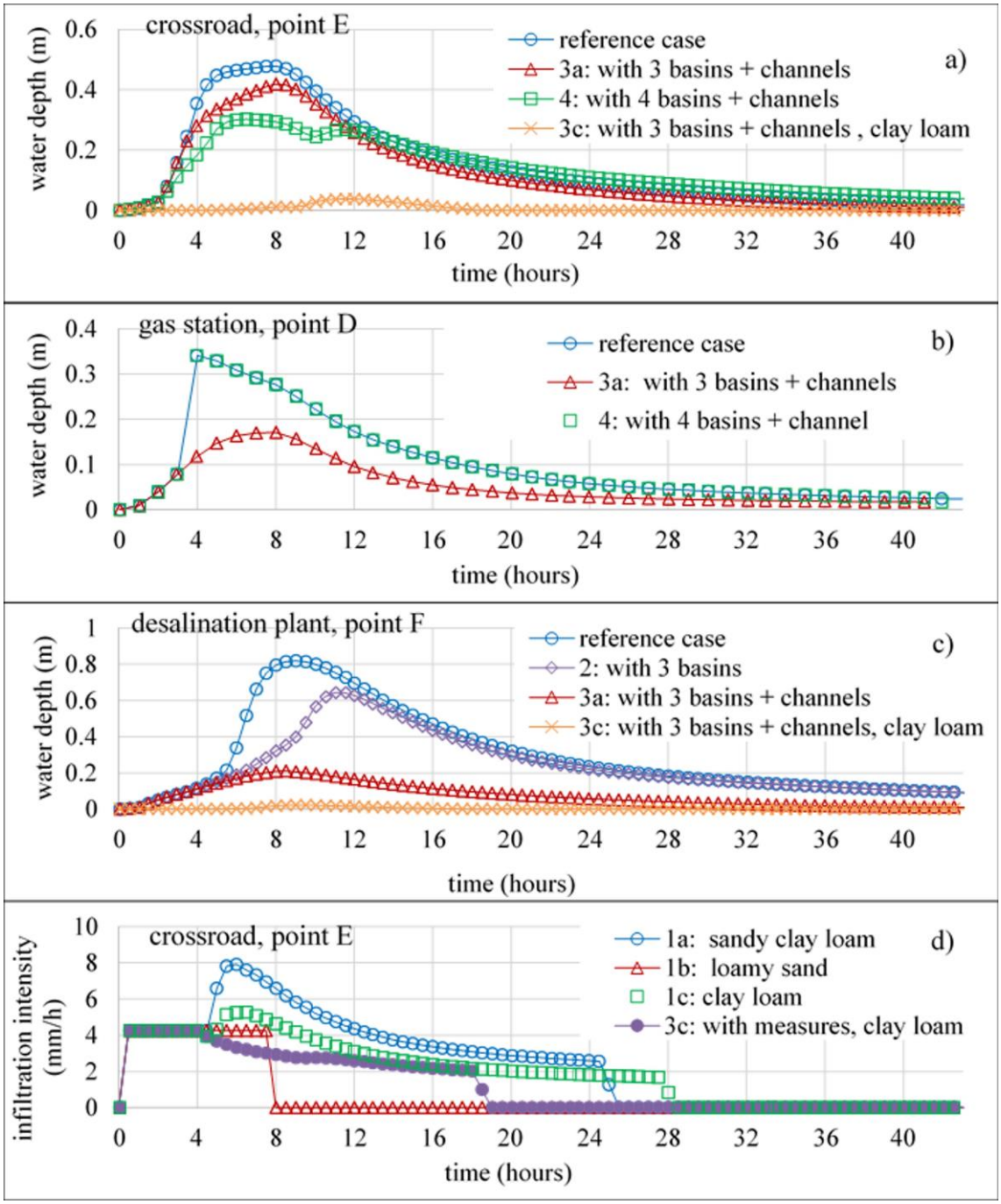

Figure 6: Water depth over time at locations close to the a) crossroad, b) the gas station and c) the desalination plant (points E, D and F in Figure 3b) for different scenarios of mitigation measures or the combination of mitigation measures with infiltration, and infiltration rates for different soils or the combination of infiltration and mitigation measures in d)

3.3.3. Worst case scenario with increased rainfall intensity

In the scenarios 1d, 1e, 3c and 3d, a very strong rainfall event of 90 mm of accumulated rainfall over the whole Wadi Bili catchment was taken into account to investigate the impact of an exceptional flood event and the effectiveness of the chosen mitigation measures fur such situation. The input hydrograph for this event was created by a hydrological catchment model by using the Software STORM (Sieker, 2019). The model was set-up for the Wadi Bili catchment and calibrated to the runoff measurements of Hadidi (2016). Furthermore, the local rainfall inside the model area of El Gouna was also increased to a rainfall intensity of 11.25 mm/h over 8 hours leading to 90 mm accumulated rainfall. Figure 7 shows the water depths after 9 hours for the four different scenarios. In 1d and 1e, the flood wave together with the local rain lead to large inundated areas with very high water depths up to 2 m around the desalination plant (point F in Figure 7a). The difference between the scenarios with and without infiltration is almost not visible, which indicates that the infiltration plays a less important role with increasing floods. In scenario 3c different aspects of the impact of the mitigation measures can be observed. On the one hand, the flooding around the desalination plant (point F in Figure 7a) could be successfully reduced in terms of flooded areas and water depths, from 2 m without measures to 55 cm (73 %) and even 28 cm (86 %) when infiltration was considered (Figure 8a). On the other hand, even higher water depths occurred at other locations as for example around the gas station (point D in Figure 7a) northeast of the biggest retention basin. This should be explained by the fact that the retention basin is overflowing in the northeast corner, because the water elevation becomes higher than the natural bottom surface. The outflow at this location propagates with very high velocities in northeast direction generating inundations of up to 1.50 m along the main road and 1.22 m close to the gas station

(point D in Figure 7a), while in the scenario without mitigation measures the water depths at the same locations are around 0.87 m and 0.77 m, respectively (Figure 8b). At these locations, the failure of the measures leads to an increase in water depth by 72 % and 58 %, respectively, compared to the case without any measures. Similar effects can be observed directly east of the retention basin 2, where the water depth with mitigation measures is about 10 cm higher than without mitigation measures. Therefore, it can be concluded that the dimensions of the retention basins would not be sufficient for such an exceptional extreme event.

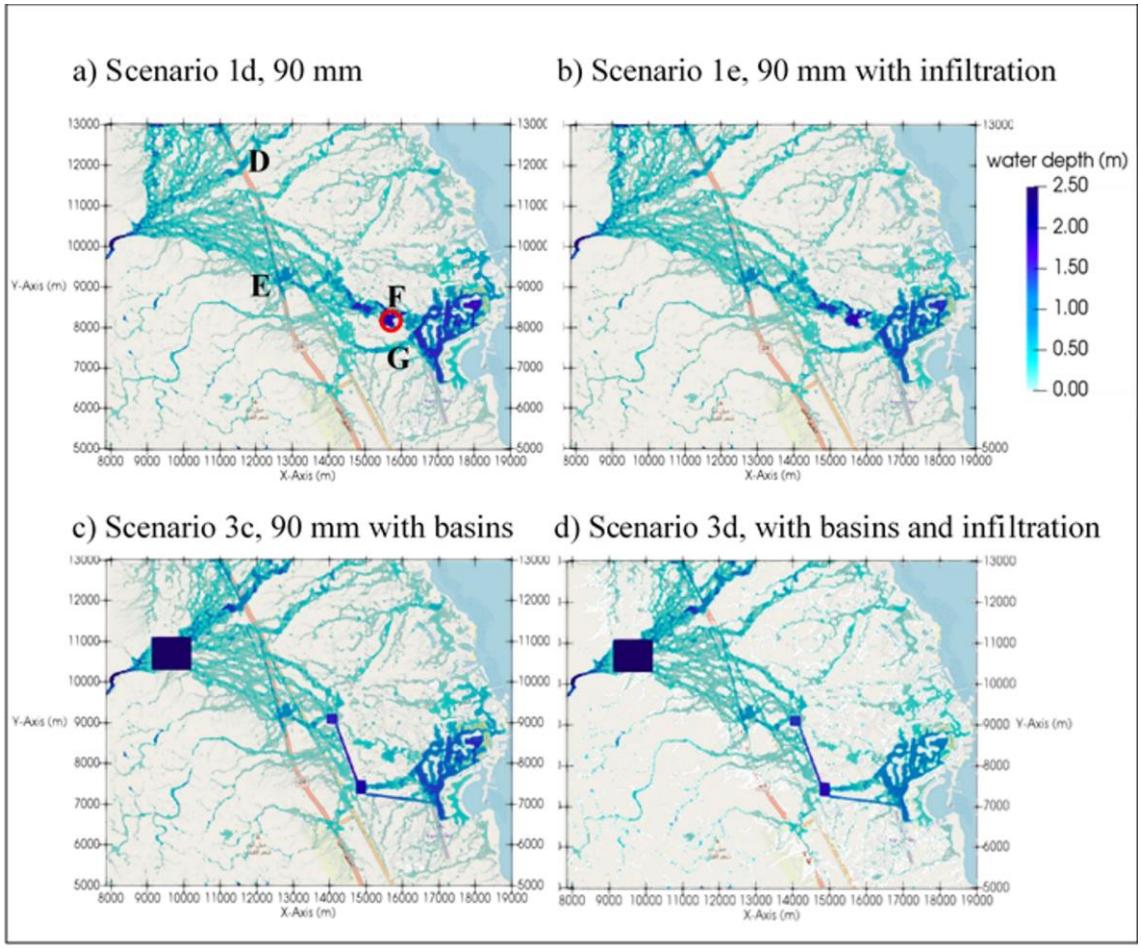

Figure 7: Water depths after 9 hours for different scenarios with and without mitigation measures and infiltration for the exceptional extreme event of 90 mm of accumulated rainfall, plotted on www.openstreetmap.org ©OpenStreetMap contributors

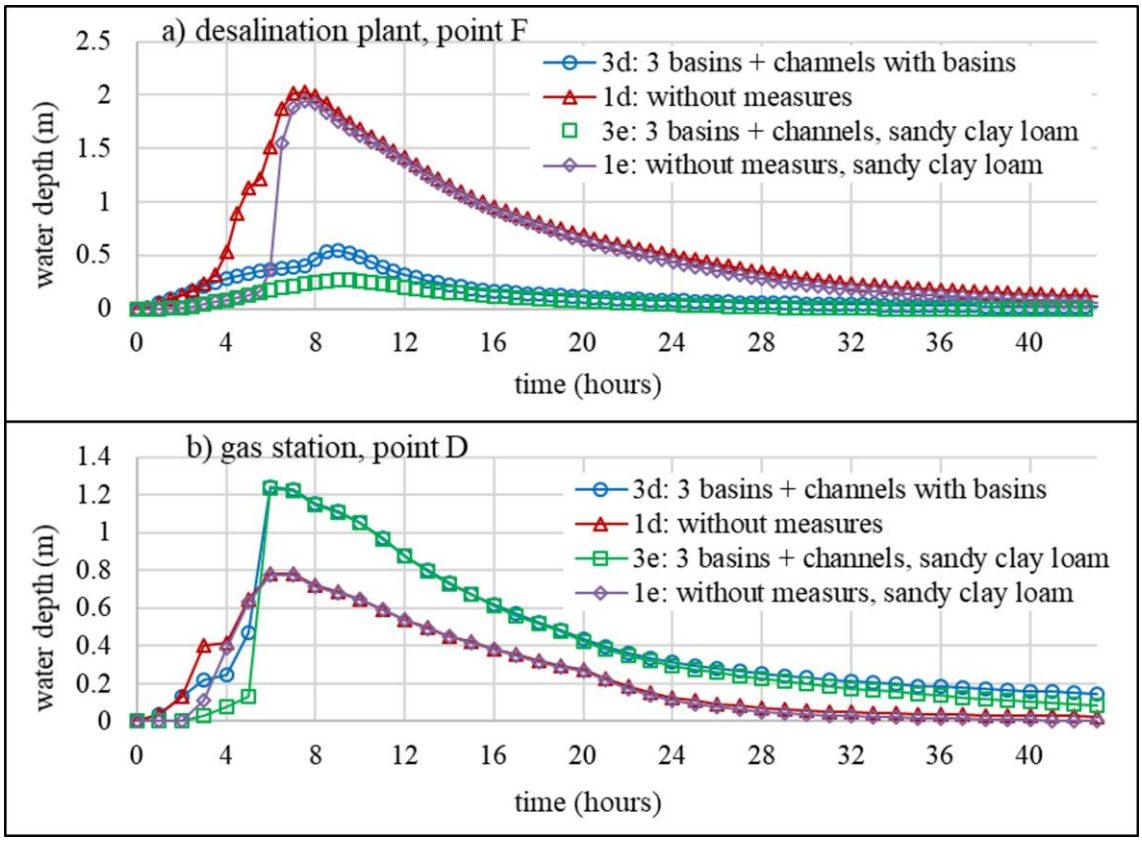

Figure 8: Temporal development of the water depth for different scenarios with and without mitigation measures and infiltration for the exceptional extreme event of 90 mm of accumulated rainfall, at the location close to the desalination plant (a) and next to the gas station (b)

3.4 Discussion of results

The consideration of loamy sand lead to a clear overestimation of infiltration. The consideration of sandy clay loam with the tabled Green-Ampt parameters also showed an overestimation, because the local rain infiltrated completely and no surface runoff occurred apart from the flood wave from Wadi Bili, although inundated areas at different location inside the city area during the event 2014 have been reported by the community. After the Harmonized World Soil Database, the dominant soil type in this area would be coarse sand (FAO, 2019). Field measurements of infiltration using a doublering infiltrometer were carried out within the study program Water Engineering of TU Campus El Gouna, and showed infiltration rates in the order of magnitude of 10^{-5} m/s at most locations inside the model domain. Only at a few locations clayey soils have been observed and at one location an infiltration rate of $7 \cdot 10^{-7}$ m/s was measured.

It can be concluded that infiltration is generally overestimated in the model. One reason for this could be surface clogging, which might occur during heavy rainfalls in non-vegetated arid areas such as the study area, and would lead to decreased infiltration rates (Thomas, 2011). The effect of surface clogging was not included in the model. Also, the measurement method with a doublering infiltrometer might not represent the processes appropriately, as the soil is continuously covered by a certain water depth leading to suspension of the fine sediments in the beginning, while in reality they could be aggregated due to the kinetic energy of the rain drops leading to a sealed crust with decreased infiltration capacity (Tian et al., 2017). Rainfall simulators including devices to measure infiltration rates would be a better method than the doublering infiltrometer. In some studies, such as in Fernández-Pato et al. (2016) and Simons et al. (2014), infiltration was also overestimated especially in the beginning of the rainfall event leading to a delayed beginning of overland flow. Esteves et al. (2000) used the extended Green-Ampt model, which takes into account crusted soils by using a harmonic average of hydraulic conductivities of crust and sub-crust soil to determine the effective hydraulic conductivity (Rawls et al., 1990). This approach could be adapted for the study area, while further measurements of the soil characteristics would be necessary. Other possible reasons could be sub-grid rill-flow, where the flow would occur more concentrated and faster over smaller soil surfaces leading to a reduced infiltration, which is also indicated in the investigations of Kuhn &Yair (2004). Furthermore, the reduced infiltration capacities of the urban structures have not been considered. The impact of spatially variable infiltration rates considering especially the low hydraulic conductivity of urban areas is currently under investigation within the scope of a bachelor thesis.

4. Conclusions and Outlook

Different mitigation strategies and infiltration scenarios have been investigated with a robust 2D shallow water model for the region of El Gouna in Egypt. The presented measures are examples to illustrate, how the model can help to define appropriate locations and dimensions of mitigation measures. Furthermore, the following conclusions should be pointed out:

- Infiltration should not be neglected during rainfall-runoff simulations in arid areas with natural soils, as the dry conditions and the hydraulic conductivity of natural and often sandy soils lead to a significant effect of infiltration in terms of reduced water depths and delayed flood peaks.
- Only in the case of exceptional events as shown in the last example of this study, the impact of infiltration becomes less important.
- Mitigation measures are much more effective when infiltration is considered, as the combined effect of retention and diverting water (through mitigation measures) and infiltration is much bigger than the single effects.
- Retention basins combined with drainage channels lead to a much more effective mitigation than without drainage channels.
- Besides flood mitigation, the measures can be combined with the direct usage or artificial recharge as they enhance increased infiltration at specified locations. Therefore, detailed knowledge of subsurface conditions as well as methods to prevent surface clogging must be taken into account.
- Mitigation measures should be carefully investigated in advance and with consideration of the overall domain, because they may have contrary effects when being overstrained and leading to increased risk of flooding in some areas, while they successfully reduce the flooding at other areas.

The limits of the applicability of the presented model are reflected in the general overestimation of infiltration. Different reasons, which could be responsible for this effect, have been discussed and should be further studied, such as:

- Surface clogging due to fine sediments
- Sub-grid rill flow leading to a faster flow over smaller areas resulting in less infiltration
- Relatively coarse resolution of the DEM and neglecting low permeable urban surfaces
- Method of doublering infiltrometer not appropriate, rainfall simulators should be used instead.

Acknowledgements

The work was supported by TU Berlin, Germany. The travel grants of the DFG Research Training Group “Urban Water Interfaces” are gratefully acknowledged.

Disclosure statement

No potential conflict of interest was reported by the authors.

References

Bauer, F., Hadidi, A., Tügel, F. and Hinkelmann, R., 2019. Flash Flood Investigations in El Gouna, Northern Red Sea Governorate. In: A. M. Negm, ed. *Flash Floods in Egypt.*Springer, Forthcoming. Springer International Publishing, Basel.

Blöschl, G. & Sivapalan, M., 1995. Scale Issues in Hydrological Modelling: A Review. *Hydrological Processes,* Issue 9, pp. 251-290.

Burle, S., 2018. *floodmap.net.* [Online]

Available at: http://www.floodmap.net/Elevation/ElevationMap/?gi=6692512

[Zugriff am 10 05 2019].

Esteves, M., Faucher, X., Galle, S. & Vauclin,, M., 2000. Overland flow and infiltration modelling for small plots during unsteady rain: numerical results versus observed values. *Journal of Hydrology,* 228(3–4), pp. 265-282.

FAO, 2019. *Harmonized World Soil Database v 1.2.* [Online]
Available at: http://www.fao.org/soils-portal/soil-survey/soil-maps-and-databases/harmonized-world-soil-database-v12/en/
[Accessed 17 01 2019].

Fernández-Pato, J., Caviedes-Voullième, D. & García-Navarro, P., 2016. Rainfall/runoff simulation with 2D full shallow water equations: Sensitivity analysis and calibration of infiltration parameters. *Journal of Hydrology,* Band 536, pp. 496-513.

Gargouri-Ellouze, E. & Eslamian, S., 2014. Application of Copulas in Hydrology: Geomorphological Instantaneous Unit Hydrograph and Intensity Index of Infiltration Frequency. In: S. Eslamian: *Handbook of Engineering Hydrology Ch. 1, Vol. 2: Modeling, Climate Changes and Variability,* pp. 1-18. USA: Francis and Taylor, CRC Group.

Gargouri-Ellouze, E., Eslamian, S.: Ostad-Ali-Askari, K., Chérif, R., Bouteffeha, M. & Slama, F., 2017. Infiltration. In: M. B. Bobrowsky P.: *Encyclopedia of Engineering Geology,* pp. 513-514 Encyclopedia of Earth Sciences Series, Springer, Cham.

Hadidi, A., 2016. *Wadi Bili Catchment in the Eastern Desert - Flash Floods, Geological Model and Hydrogeology, Dissertation.* Berlin: Fakultät VI – Planen Bauen Umwelt der Technischen Universität Berlin.

Hou, J., Liang, Q., Simons, F. & Hinkelmann, R., 2013. A Stable 2D Unstructured Shallow Flow Model for Simulations of Wetting and Drying over Rough Terrains. *Computers & Fluids*, p. 132–147.

Kuhn, N. J. & Yair, A., 2004. Spatial distribution of surface conditions and runoff generation in small arid watersheds, Zin Valley Badlands, Israel. *Geomorphology*, Band 57, pp. 183-200.

Marafini, E., 2017. *Investigation of Mitigation Measures against Wadi Flash Floods.* Rome: Ingegneria Civile per la Protezione dai Rischi Naturali Idraulica - Roma Tre, Università degli studi.

Marafini, E., Tügel, F. Özgen, I., Hinkelmann, R. & La Rocca, M., 2018. Flash Flood Simulations Based on Shallow Water Equations to Investigate Protection Measures for El Gouna, Egypt. In: *13th International Conference on Hydroinformatics.* Palermo

Merkel, A., 2019. *climate-data.org.* [Online]

Available at: https://en.climate-data.org/africa/egypt/red-sea-governorate/hurghada-415 [Zugriff am 10 05 2019].

Murillo, J., García-Navarro, P. & Burguete, J., 2009. Conservative Numerical Simulation of Multi-Component Transport in Two-Dimensional Unsteady Shallow Water Flow. *Journal of Computational Physics*, Volume No. 15, p. 5539–5573.

Rawls, W., Brakensiek, D. & Miller, N., 1983. Green-Ampt Infiltration Parameters from Soils Data. *Journal of Hydraulic Engineering*, Volume 1, pp. 62-70.

Rawls, W. J., Brakensiek, D. L., Simanton, J. R. & Kohl, K. D., 1990. Development of a Crust Factor for a Green Ampt Model. *Transactions of the ASAE,* 33(4), pp. 1224-1228.

Sieker, 2019. *STORM XXL*. [Online]

Available at: https://www.sieker.de/de/software/downloads/download/stormxxl-deutsch-2.html.

Simons, F., Busse, T., Hou, J.; Özgen, I. & Hinkelmann, R., 2014. A Model for Overland Flow and Associated Processes within the Hydroinformatics Modelling System. *Journal of Hydroinformatics*, Vol. 16(No. 2), p. pp 375–391.

Singh, J., Altinakar, M. S. & Ding, Y., 2015. Numerical Modeling of Rainfall-Generated Overland Flow Using Nonlinear Shallow-Water Equations. *Journal of Hydrologic Engineering*, 20(8).

Thomas, D. S. G., 2011. *Arid Zone Geomorphology: Process, Form and Change in Drylands.* John Wiley & Sons, , Chichester.

Tian, P., Xu, X., Pan, C., Hsu, K. & Yang, T., 2017. Impacts of rainfall and inflow on rill formation and erosion processes on steep hillslopes. *Journal of Hydrology* , Band 548, pp. 24-39.

Whisler, F. & Bouwer, H., 1970. Comparison of Methods for Calculating Vertical Drainage and Infiltration for Soils. *Journal of Hydrology*, Issue 1, pp. 1-19.

Xing, Y., Liang, Q., Wang, G., Ming, X. & Xia, X., 2019. City-scale hydrodynamic modelling of urban flash floods: the issues of scale and resolution. *Naturzal Hazards*, 96(473).